Disease-causing mutation in α-actinin-4 promotes podocyte detachment through maladaptation to periodic stretch

Di Feng[a,b], Jacob Notbohm[c], Ava Benjamin[a,b], Shijie He[d], Minxian Wang[a,b], Lay-Hong Ang[b,e], Minaspi Bantawa[f], Mehdi Bouzid[f], Emanuela Del Gado[f], Ramaswamy Krishnan[b,g,1], and Martin R. Pollak[a,b,1,2]

[a]Division of Nephrology, Department of Medicine, Beth Israel Deaconess Medical Center, Boston, MA 02215; [b]Harvard Medical School, Boston, MA 02215; [c]Department of Engineering Physics, University of Wisconsin–Madison, Madison, Wisconsin, WI 53706; [d]Department of Environmental Health, Harvard T. H. Chan School of Public Health, Boston, MA 02115; [e]Confocal Imaging Core, Beth Israel Deaconess Medical Center, Boston, MA 02215; [f]Department of Physics, Institute for Soft Matter Synthesis and Metrology, Georgetown University, Washington, DC 20057; and [g]Department of Emergency Medicine, Beth Israel Deaconess Medical Center, MA 02215

Contributed by Martin R. Pollak, December 29, 2017 (sent for review October 13, 2017; reviewed by Wilhelm Albert Kriz and Dimitrije Stamenovic)

α-Actinin-4 (ACTN4) bundles and cross-links actin filaments to confer mechanical resilience to the reconstituted actin network. How this resilience is built and dynamically regulated in the podocyte, and the cause of its failure in ACTN4 mutation-associated focal segmental glomerulosclerosis (FSGS), remains poorly defined. Using primary podocytes isolated from wild-type (WT) and FSGS-causing point mutant Actn4 knockin mice, we report responses to periodic stretch. While WT cells largely maintained their F-actin cytoskeleton and contraction, mutant cells developed extensive and irrecoverable reductions in these same properties. This difference was attributable to both actin material changes and a more spatially correlated intracellular stress in mutant cells. When stretched cells were further challenged using a cell adhesion assay, mutant cells were more likely to detach. Together, these data suggest a mechanism for mutant podocyte dysfunction and loss in FSGS—it is a direct consequence of mechanical responses of a cytoskeleton that is brittle.

kidney | podocyte | cytoskeleton | α-actinin-4 | actin

Podocytes are an essential component of the kidney glomerular filtration barrier, maintaining its structural integrity and regulating the slit diaphragm through cellular contractile forces (1–3). Podocyte contraction is mediated by the actin cytoskeleton connected by cross-linking proteins, including α-actinin-4 [ACTN4 (human gene or protein); Actn4 (mouse gene or protein)]. Mutations in the actin-binding domain of ACTN4 cause podocyte dysfunction and progressive kidney disease in humans (4). All of the disease-causing mutations localize to the actin-binding domain of ACTN4 and increase the binding affinity between ACTN4 and actin filaments in vitro (4–7). The biophysical properties of this actin network are sensitive to changes in the binding affinity of ACTN4 to F-actin (8). Studies using reconstituted actin filaments show that mutant ACTN4 stiffens and solidifies the actin network (8, 9). Mutant ACTN4 makes the actin network more brittle with a lower breaking strength (9). While these biophysical measurements provide insight into how mutant ACTN4 affects the actin cytoskeleton in vitro, how they contribute to podocyte dysfunction and in vivo biophysical changes remains unclear.

Podocytes in vivo are routinely stretched due to expansion–retraction of glomerular capillaries (10, 11). In response to stretch, podocytes reorganize their cytoskeleton (12–14). Studies have shown complex intrapodocyte signaling cascades, including calcium influx, induced by stretch (13, 15). Cells across a wide range of organs including lung, bladder, and blood vessels, respond by promptly ablating and then slowly restoring their contraction consistent with the physical mechanisms of fluidization and resolidification (16–20). This fluidization–resolidification process appears to be mediated by actin disruption and repair (16, 19).

We studied primary podocytes isolated from wild-type (WT) and homozygous mutant Actn4 knockin ($Actn4^{K256E/K256E}$) mice. We used cell-mapping rheometry to impose periodic stretch (16, 17, 19) and traction force microscopy (21) to map the spatiotemporal changes in contraction, manifested as traction on the substrate. These tractions must be balanced by intracellular stress (22–27) that we quantified using stress microscopy (25, 28). Under stretch, mutant podocytes showed impaired recovery of contraction and irreparable breakages in their actin cytoskeletons, akin to breaking of a brittle cytoskeleton. This failure was directly attributable to the ability of the Actn4 mutation to induce a stiffer and more spatially aligned cytoskeleton as well as to enhance spatial correlation of intracellular stress. Taken together, our findings suggest a mechanism by which mutant Actn4 disrupts the internal biomechanics of the podocyte, leaving it vulnerable to detachment when faced with the mechanical challenges of its environment.

Results

Mutant Podocytes Fail to Recover Their Contraction After Periodic Stretch. We used CRISPR/Cas9 technology to generate a point mutant Actn4 K256E mouse model. This model was developed to avoid potential confounding issues with earlier models, including an impure genetic background, and the presence of an

Significance

Point mutations in α-actinin-4 (ACTN4) cause a form of kidney disease in humans. Although we know these mutations affect kidney podocytes, the mechanism by which they lead to podocyte dysfunction remains unclear. Here, we show that homozygous mutant Actn4 podocytes developed irrecoverable reductions in their contraction and irreparable disruptions in their actin cytoskeletons when subjected to periodic stretch. This maladaptive response is akin to failure of a brittle material under deformation. Our results clarify the mechanism by which mutations in ACTN4 leave the podocyte more vulnerable to detachment in the progression of kidney disease.

Author contributions: D.F., R.K., and M.R.P. designed research; D.F., A.B., and L.-H.A. performed research; J.N., S.H., M.W., M. Bantawa, M. Bouzid, and E.D.G. contributed new reagents/analytic tools; D.F., E.D.G., R.K., and M.R.P. analyzed data; and D.F., R.K., and M.R.P. wrote the paper.

Reviewers: W.A.K., University of Heidelberg; and D.S., Boston University.

The authors declare no conflict of interest.

[1]R.K. and M.R.P. contributed equally to this work.

[2]To whom correspondence should be addressed. Email: mpollak@bidmc.harvard.edu.

This article contains supporting information online at www.pnas.org/lookup/suppl/doi:10.1073/pnas.1717870115/-/DCSupplemental.

intronic LoxP site (29, 30). These homozygous Actn4 knockin ($Actn4^{K256E/K256E}$) mice developed both albuminuria and podocyte loss (Fig. S1) at 4–7 wk of age. These cells allow (*i*) the study of mutant and WT Actn4 under the control of the endogenous regulatory machinery rather than an overexpression system and (*ii*) the study of Actn4 in primary podocytes freshly isolated from glomeruli.

We subjected individual WT and $Actn4^{K256E/K256E}$ podocytes to equibiaxial stretches (10% in magnitude and 4 s in duration, spaced 3 min apart) using previously described methods (16, 17, 19, 20). Contractile moment (a scalar measure of overall cell contraction) was measured before (Fig. 1*A* and Fig. S5) and after stretch across several time points and normalized by each cell's baseline value (Fig. 1*B*). Immediately after the first stretch, podocytes in both groups acutely ablated their contraction to a similar extent [WT median (interquartile range), 41% (35–47%), vs. $Actn4^{K256E/K256E}$, 43% (40–53%)], consistent with cytoskeletal fluidization. However, during the recovery period, $Actn4^{K256E/K256E}$ podocytes were only able to recover 63% of their baseline contraction [63% (2–82%)], whereas WT podocytes recovered greater than 84% of their baseline value [84% (80–90%)], consistent with cytoskeletal resolidification. After the second and third transient stretches, $Actn4^{K256E/K256E}$ podocytes failed to recover their contraction to the same extent as the WT [WT, 75% (66–80%), vs. $Actn4^{K256E/K256E}$, 20% (0–65%) after the second stretch, and 78% (68–83%) vs. $Actn4^{K256E/K256E}$, 26% (0–57%) after the third stretch]. The spreading area of both WT and $Actn4^{K256E/K256E}$ podocytes remained relatively constant throughout the periodic stretches (Fig. S2). These findings show that the response of WT podocytes to periodic stretch is consistent with fluidization–resolidification (16), whereby WT podocytes ablated their contraction with each stretch but were able to restore the majority of their baseline value. In contrast, $Actn4^{K256E/K256E}$ podocytes on average deviated from this homeostasis, particularly in the ability to restore their baseline contraction in between stretches.

We next examined structural changes in the actin cytoskeleton that might correspond to the contraction changes reported above. We transfected podocytes with a fluorescent actin marker (LifeAct) (*Materials and Methods*) to observe differences in actin

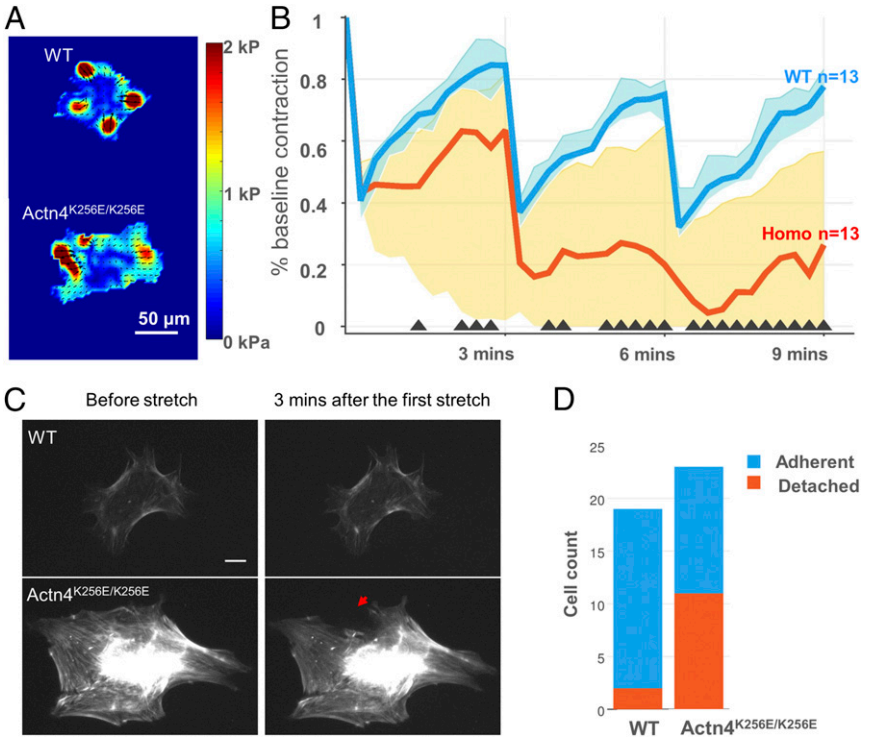

Fig. 1. In response to repeated stretch, the $Actn4^{K256E/K256E}$ podocytes failed to recover their contraction, developed irreparable disruptions in their actin cytoskeleton, and detached at a higher rate. (*A*) Representative traction force maps for WT and $Actn4^{K256E/K256E}$ podocytes. Different colors correspond with different magnitudes of traction, with red corresponding to the highest magnitude. Arrows indicate direction of traction. (Scale bar: 50 μm.) (*B*) Single-podocyte contraction dynamics in response to three transient stretches over time. A custom-designed stretch device was used to superimpose a 4-s, 10% transient stretch (followed by release) onto individual WT and $Actn4^{K256E/K256E}$ podocytes adherent to a 26-kPa substrate. The *y* axis plots individual podocyte contractile forces, assessed by the contractile moment, normalized by their baseline value before stretch, while the *x* axis plots serial time points relative to the three transient stretches. Graphed values represent the median (lines) and interquartile ranges (shaded areas). Black triangles along the *x* axis indicate time points where there is a significant difference between WT and mutant ($P < 0.01$). Compared with WT podocytes ($n = 13$), $Actn4^{K256E/K256E}$ podocytes ($n = 13$) showed decreasing contraction after three stretches, with a median recovery of only 26% of their initial contraction, whereas WT podocytes maintained over 78% of their baseline contraction at 9 min (final time point). Data were pooled from five separate independent experiments. (*C*) In response to stretch, $Actn4^{K256E/K256E}$ podocytes showed breakages in their actin structure after stretch that failed to recover. Representative 20× images of actin filaments of actin of WT (*Upper*) and $Actn4^{K256E/K256E}$ (*Lower*) podocytes before and after one stretch cycle. $Actn4^{K256E/K256E}$ podocytes demonstrated visible cytoskeletal breakages after stretch that did not repair during the 3-min recovery period (red arrow), whereas WT podocytes demonstrated small areas of actin breakages that were largely repaired. (Scale bar: 20 μm.) Time-lapse images are shown for WT in Movie S1 and $Actn4^{K256E/K256E}$ in Movie S2. (*D*) After repeated stretches, $Actn4^{K256E/K256E}$ podocytes were more likely to detach from their substrates than WT when subjected to a spinning-disk detachment assay. Blue indicates the number of cells that remain adherent to their substrate after three stretches, and red indicates the number of cells that detached from their substrate after three stretches. The cell count was pooled from four separate independent experiments. Only 2 of 19 (11%) WT podocytes detached from their substrate after three stretches, whereas 11 of 23 (48%) mutant podocytes detached (odds ratio, 7.42; 95% CI, 1.27, 80.75; $P = 0.017$).

cytoskeleton structural integrity between WT and Actn4$^{K256E/K256E}$ podocytes in response to periodic stretch under identical experimental conditions as in the case of traction force measurements (Fig. 1*C*). In response to the first stretch cycle, both WT and mutant podocytes displayed clear evidence of actin disruption (Movies S1 and S2). While these disrupted regions largely recovered in WT cells, they persisted in mutant cells.

Mutant Podocytes Are More Likely to Detach After Periodic Stretch. Since contractile forces are required for cell adhesion (31), the failure of mutant podocytes to recover their contraction after stretch may have a direct consequence on podocyte attachment. A separate group of WT and Actn4$^{K256E/K256E}$ podocytes were subjected to three 10% stretches of 4-s duration. After the 3-min recovery period following the third and final stretch, both groups of cells underwent a spinning-disk detachment assay (*Materials and Methods*). We used nuclear staining to quantify cells before and after spin, and used the difference between these values to determine the number of cells that detached after spin. As shown (Fig. 1*D*), among all cells studied (pooled from four independent experiments), mutant podocytes (11/23) had a higher probability of detachment than WT (2/19) (odds ratio, 7.42; 95% CI, 1.27, 80.75; $P = 0.017$).

Mutant Podocytes Bear More Spatially Correlated Intracellular Stress. What makes the mutant podocyte more vulnerable to periodic stretch? To determine whether there were changes in the mutant podocytes that predisposed them to failure, we compared their baseline physical characteristics with WT cells. Given that we observed actin disruption to correspond with Actn4$^{K256E/K256E}$ podocytes' impaired recovery after stretch, we first looked at changes in the actin filaments that resulted from mutant Actn4 using phalloidin to stain the actin within both groups of cells seeded on a collagen-coated coverslip (Fig. S3). We found that Actn4$^{K256E/K256E}$ podocytes exhibited more elongated and well-developed stress fibers than WT (Fig. 2*A*), consistent with previous reports (19). Additionally, we observed that the stress fibers in Actn4$^{K256E/K256E}$ podocytes appeared to be aligned more parallel to each other than the actin filaments distributed in WT. We used previously described methods to measure the relative alignment of actin filaments using the autocorrelation function (*Materials and Methods*) (32). The autocorrelation function [$C(r)$] measures the orientation of actin filaments and correlates these orientations over space. More alignment across the cell yields higher autocorrelation [$C(r)$ closer to 1] than random orientation. As shown in Fig. 2*B*, the actin filaments across Actn4$^{K256E/K256E}$ cells were more aligned than the actin filaments in WT consistent with our visual impression. Finally, these structural differences in Actn4$^{K256E/K256E}$ cells were accompanied by a significantly enhanced cytoskeletal stiffness (Fig. S4).

Because a prominent role of actin filaments is to bear intracellular stress (33), we compared baseline intracellular stress between WT and Actn4$^{K256E/K256E}$ podocytes (25, 28, 34). We computed the intracellular stress from the traction measurements (Fig. S5). We separated intracellular stress into two constituent components: we report the magnitude of mean principal stress as tension (σ), and the orientation of first principal stress as principal orientation (θ) (25, 28, 34). We first looked at the mean intracellular tension of the entire cell $\bar{\sigma}$ (Fig. S5). We found that for cells seeded on 26-kPa gel, the mean tension $\bar{\sigma}$ was not statistically different between WT and Actn4$^{K256E/K256E}$ podocytes [WT median (interquartile range), 1,147 ± (880–1,577) Pa, vs. Actn4$^{K256E/K256E}$, 1,675 ± (946–2,240) Pa]. To determine how intracellular stress varies across the cell, we calculated the spatial distribution of both σ and θ using an autocorrelation function (similar to that used for the orientation of actin filaments above). The more spatially aligned the intracellular tension and its principal orientation, the higher the

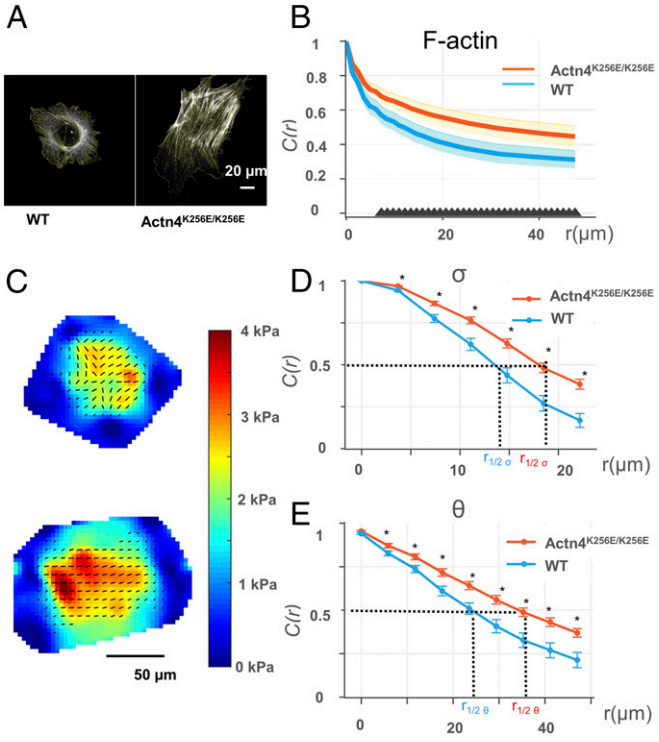

Fig. 2. Podocytes of Actn4$^{K256E/K256E}$ mice exhibit more correlated actin filament orientation and intracellular stress. (*A*) Representative 63× images of actin filaments in a WT (*Upper*) and an Actn4$^{K256E/K256E}$ (*Lower*) podocyte grown on a collagen-coated coverslip. (Scale bar: 20 μm.) Light yellow lines indicate the average of the angles of actin filament vectors within a region of 10 × 10 pixels (1 px = 0.19 μm). (*B*) Quantification of the distribution of actin filament orientation across WT and Actn4$^{K256E/K256E}$ podocytes. This quantification was calculated by the autocorrelation function $C(r)$ (y axis), which is a measure of the correlation, or uniformity, of actin filament orientation over increasing distances across the cell (x axis). The closer to a value of 1, the more correlated, or uniform, the actin filament orientation between any two given regions of 10 × 10 pixels. Data were obtained from nine WT and nine Actn4$^{K256E/K256E}$ podocytes grown on a collagen-coated coverslip and plotted as median (lines) and interquartile ranges (shaded areas). At increasing distances across the cell, Actn4$^{K256E/K256E}$ podocytes maintain more spatially correlated actin filament orientation than WT. The black triangles along the x axis indicate distances where the median autocorrelation between Actn4$^{K256E/K256E}$ podocytes and WT are significantly different ($P < 0.05$). (*C*) Representative intracellular stress maps of WT (*Upper*) and Actn4$^{K256E/K256E}$ (*Upper*) podocytes grown on 26-kPa substrates. For the intracellular stress maps, red indicates the greatest magnitude of mean principal stress. The black lines represent the local intracellular stress both in terms of tension (σ, corresponding to length of the line) and orientation (θ, corresponding to orientation of the line). (Scale bar: 50 μm.) (*D*) Quantification of the distribution of σ across WT and Actn4$^{K256E/K256E}$ podocytes. As above, y axis plots the autocorrelation function $C(r)$ of σ, and the x axis plots distance across the cell. At increasing distances across the cell, Actn4$^{K256E/K256E}$ podocytes maintain more spatially correlated, or more uniformly distributed, σ than WT. The black asterisk (*) along the x axis indicate distances where the median $C(r)$ of σ between Actn4$^{K256E/K256E}$ podocytes and WT are significantly different ($P < 0.05$). (*E*) Quantification of the distribution of σ across WT and Actn4$^{K256E/K256E}$ podocytes. As above, y axis plots the autocorrelation function $C(r)$ of θ, and the x axis plots distance across the cell. At increasing distances across the cell, Actn4$^{K256E/K256E}$ podocytes maintain more spatially correlated θ than WT. The black asterisk (*) along the x axis indicate distances where the median $C(r)$ of θ between Actn4$^{K256E/K256E}$ podocytes and WT are significantly different ($P < 0.05$). For both *D* and *E*, the distance over which the $C(r)$ decays to a value of 0.5 was extrapolated as a singular value from the autocorrelation curves of each individual cell; this value is termed correlation length $r_{1/2\ \sigma}$ and $r_{1/2\ \theta}$. The greater the $r_{1/2}$ value, the greater the distance over which intracellular stress maintains uniformity in its tension ($r_{1/2\ \sigma}$) and its orientation ($r_{1/2\ \theta}$).

CELL BIOLOGY

autocorrelation, that is, $C(r)$ is closer to 1. Just as Actn4$^{K256E/K256E}$ podocytes demonstrated more aligned actin filaments, Actn4$^{K256E/K256E}$ podocytes demonstrated more aligned σ (Fig. 2*D*) and θ (Fig. 2*E*) across the cell than WT.

Does the extent of spatial correlation in σ and θ explain cell-to-cell variability in mutant stretch responsiveness (Fig. 1*B*)? We examined the autocorrelation curves of σ and θ on a cell-by-cell basis as the correlation distance, or $r_{1/2}$. We found that the more spatially correlated the σ (Fig. 3*A*) and the θ (Fig. 3*B*) across the cell at baseline, the more impaired the recovery of baseline contraction 3 min after the final stretch ($R^2 = 0.58$, $P < 0.001$; $R^2 = 0.43$, $P < 0.001$, respectively). Notably, there were a minority of mutant podocytes that resolidified similar to WT in response to stretch. In these mutants, both σ and θ were less correlated (Fig. 3 *A* and *B*). We next stratified Actn4$^{K256E/K256E}$ podocytes into those that recovered greater than 50% of their baseline contraction after three periodic stretches (Actn4$^{K256E/K256E}$ group 1, $n = 5$) and those that did not (Actn4$^{K256E/K256E}$ group 2, $n = 8$), assessing whether there were differences in the baseline distribution of intracellular stress between these two groups alongside WT podocytes ($n = 13$, all of which recovered the majority of their baseline contraction). We found that the Actn4$^{K256E/K256E}$ group 2 podocytes demonstrated a significantly more correlated σ and θ at baseline than both Actn4$^{K256E/K256E}$ group 1 and WT (Fig. 3). Interestingly, Actn4$^{K256E/K256E}$ group 2 podocytes showed progressive reduction in the correlation of σ and θ after repeated stretches, whereas Actn4$^{K256E/K256E}$ group 1 and WT maintained their baseline values (Fig. 3).

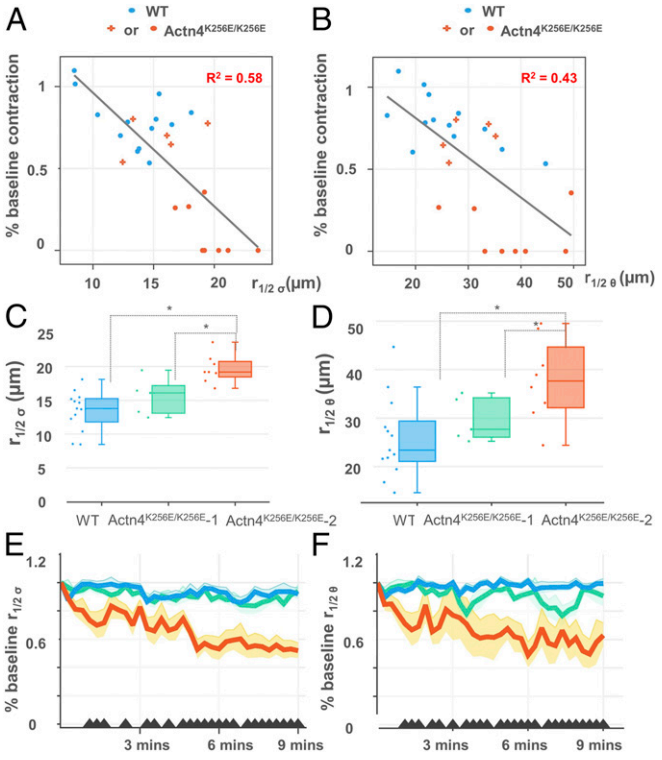

Fig. 3. More spatially correlated intracellular stress is associated with impaired contractile recovery after stretch. (*A*) Baseline $r_{1/2\ \sigma}$ (derivation described at end of Fig. 2) and (*B*) baseline $r_{1/2\ \theta}$ were inversely correlated with the final percentage of baseline contraction after the third stretch at the final time point, that is, at 9 min ($R^2 = 0.58$ and 0.43, respectively). Red points indicate the mutant podocytes that failed to recover greater than 50% of their baseline contraction (Actn4$^{K256E/K256E}$-2, $n = 8$). Red crosses indicate the mutant podocytes that were able to recover more than 50% of their baseline forces (Actn4$^{K256E/K256E}$-1 $n = 5$). Blue points indicate the WT podocytes (WT, $n = 13$, all of which recovered the majority of their baseline contraction). (*C* and *D*) Mutant podocytes that failed to recover greater than 50% of their baseline contraction (Actn4$^{K256E/K256E}$-2, $n = 8$, red bar) had higher average $r_{1/2\ \sigma}$ and $r_{1/2\ \theta}$ than mutant podocytes that were able to recover more than 50% of their baseline contraction (Actn4$^{K256E/K256E}$-1, $n = 5$, green bar) and WT podocytes (WT, $n = 13$). (*E* and *F*) Actn4$^{K256E/K256E}$-2 (red line) showed reductions in both baseline $r_{1/2\ \sigma}$ and $r_{1/2\ \theta}$ over time compared with the Actn4$^{K256E/K256E}$-1 (green line) and WT (blue line) podocytes, which maintained values similar to their baseline. The black triangles along the *x*-axis indicate the time points where there is a significant difference between WT and Actn4$^{K256E/K256E}$-2 ($P < 0.05$). Graphed values represent the mean (lines) and SE (shaded areas).

Discussion

ACTN4 mutations cause kidney disease in humans. Although these mutations have been found to increase the binding affinity of ACTN4 to actin and create a stiffer, more brittle protein network in vitro, it remains unclear how they impair podocytes in the pathogenesis of kidney disease. Here, we show that WT podocytes ablate and recover their contraction in response to periodic stretch, consistent with the universal response of fluidization–resolidification observed in living adherent cells (16). Actn4$^{K256E/K256E}$ podocytes showed an impaired response, specifically the recovery of contraction, which corresponded with irreparable disruptions in the actin cytoskeleton. Additionally, mutant ACTN4 podocytes were at higher risk of detachment after periodic stretch than WT. Our analysis of baseline physical differences between WT and mutant podocytes indicates that mutant ACTN4 leads to stiffer actin network as well as a more correlated distribution of actin filament orientation and intracellular stress in the podocyte. These alterations may contribute to the podocyte's vulnerability to stretch and propensity for detachment.

What is the specific contribution of (*i*) actin material properties and (*ii*) the tension it bears, in mediating mutant stretch responsiveness? Common pharmacological interventions such as Rho kinase inhibition are not ideal for answering this question because they simultaneously target both properties. Therefore, we used a computational model of a disordered network of semiflexible fibers to simulate the mechanics of the actin cytoskeleton (35). Using this model, we independently varied either the fiber bending stiffness or the network tension and, in each case, performed a simple shear test (Fig. 4). While increasing fiber stiffness predominantly favors irrecoverable bond breaking, increasing network tension, both in magnitude and correlation, predominantly favors earlier bond breaking, that is, bonds breaks at a smaller magnitude of imposed strain. In the context of the podocyte, these model results suggest that actin fiber stiffening promotes a more catastrophic brittle failure, and more spatially correlated intracellular tension can further lower the yield strain and therefore promote an earlier brittle failure.

Stretch is an important external mechanical challenge thought to contribute to podocytes detachment and progression of kidney disease (11). Glomerular hyperfiltration and expansion constantly subject in vivo podocytes to stretch (36). Furthermore, expansion of the glomerular basement membrane (GBM) stretches adherent podocyte cell bodies and foot processes. Multiphoton microscopy has allowed visualization of this GBM expansion: in the five-sixths nephrectomy podocyte injury mouse model (used to study the compensatory effect of hyperfiltration secondary to a reduction in functioning nephrons), the diameter of glomeruli capillary vessels was measured to increase by 15% (10).

Although previous work has observed changes in protein networks with mutant ACTN4, how the mutations change the podocyte's response to stretch is important in understanding the pathogenesis of ACTN4-mediated kidney disease. Yao et al. (9) applied stress to reconstituted actin networks cross-linked by

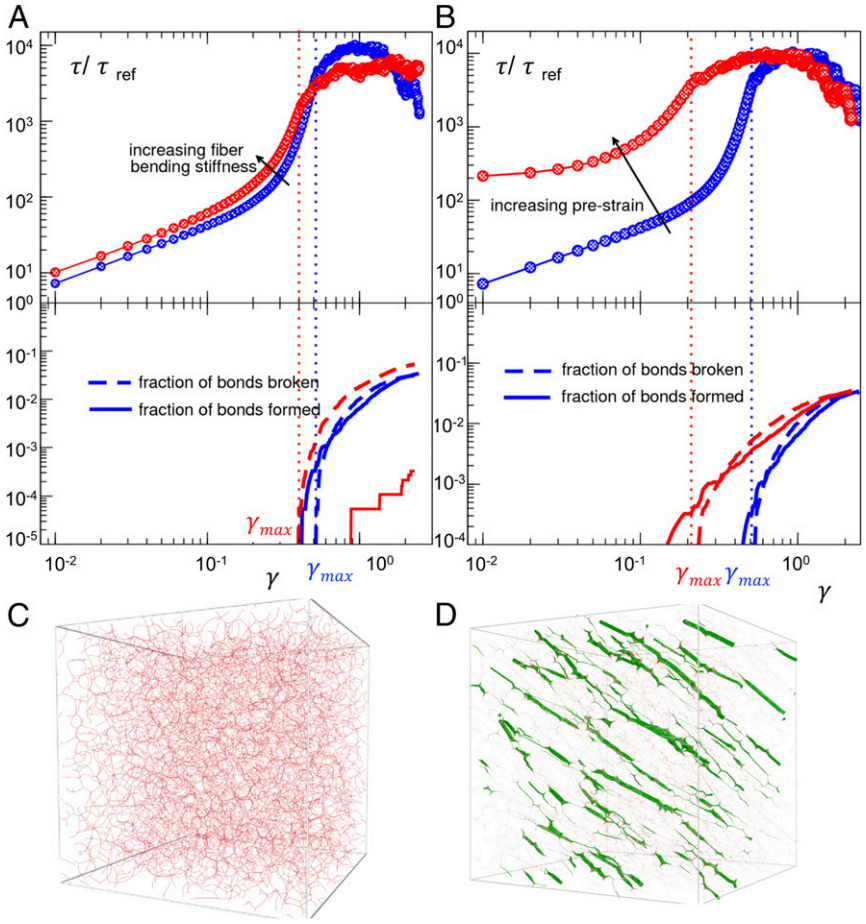

Fig. 4. Numerical simulations of model networks of semiflexible fibers subjected to a shear deformation. We have normalized by the total shear stress τ, by total shear stress τ_{ref}, the initial (small) stress of the softer material, and γ is the strain accumulated during the test. Broken bonds and newly formed bonds are shown as a function of γ in solid and dotted lines, respectively. (*A*) Increasing fiber bending stiffness lowers the yield strain. More dramatically, it lowers the capability to reform bonds as the material starts to yield. This implies a more catastrophic and brittle failure of the networks. (*B*) Increasing prestrain (as a means to increase network tension) drastically lowers the strain at which yield starts. (*C*) A simulation snapshot of the softer material used in *A* and *B* at $\gamma = 0$ (no tensile stress). (*D*) A simulation snapshot of the model material subjected to tension by applying a prestrain before the mechanical test shown in *B*. This material bears more aligned and spatially correlated tension. The thickness of the fibers is proportional to the value of the local tension in the network.

mutant ACTN4, showing that these networks were more brittle, with a lower breaking strength. Our findings in mutant podocytes are consistent with their findings in mutant protein networks: whereas WT cells appeared more able to deform and adapt to the stretch imposed upon them, mutant podocytes failed to recover their baseline structure and function, analogous to a brittle cell. Additionally, Ward et al. (8) demonstrated that actin cross-linked with mutant K255E ACTN4 created a more solid-like cytoskeletal network. Ehrlicher et al. (37) suggested that this solid-like cytoskeletal network translated into a more solid-like cell, showing that fibroblasts expressing mutant ACTN4 were less motile and more contractile than fibroblasts expressing WT ACTN4. Similarly, we found that Actn4$^{K256E/K256E}$ podocytes were stiffer and more contractile at baseline. Furthermore, the mutant ACTN4 led to a more correlated distribution of actin filament orientation and intracellular stress across the cell. More correlated intracellular stress in association with the mutation correlated with a lower recovery of baseline contraction after repeated stretch. Our findings suggest that it is not only the increased magnitude of baseline stiffness and contractile moment that is of importance but also how mutant ACTN4 redistributes intracellular stress across the podocyte.

Podocytes detach at variable rates in human and animal models of glomerular kidney disease (38–41). We found the same in Actn4$^{K256E/K256E}$ mice. We also observed variability across Actn4$^{K256E/K256E}$ podocytes in their distribution of intracellular stress and degree of impaired recovery, with a minority of mutant podocytes recovering and resisting detachment similar to WT. These findings imply that the mutation impairs podocytes in varying degrees rather than in a universal fashion. This variability in cellular phenotype in vitro may underlie the variability in podocyte detachment across glomeruli in vivo, with mutant podocytes that are less able to recover their structure and function in response to periodic stretch at risk for detaching earlier than the more resilient mutant podocytes. We note that it was not merely the distribution of intracellular stress or other physical vulnerabilities associated with the mutation that cause podocyte failure, but that these vulnerabilities required exposure to stretch to bring about dysfunction. In this light, stretch itself became pathogenic for mutant podocytes. Future studies could evaluate whether varying degrees of stretch correspond with varying degrees of failure. The varying vulnerability for impaired recovery conferred by mutant Actn4 and the varying degrees of stretch experienced within and across glomeruli could both independently contribute to an individual cell's likelihood of detachment.

We show that mutant podocytes detached at a higher rate than WT podocytes after repeated stretch. Given that a normal

contractile system within a podocyte (including actin, α-actinin, and myosin) is necessary for the podocyte to maintain adhesion to its underlying substrate (3), we speculate that the disruption of actin and the loss of baseline contraction that we observed in mutant podocytes after stretch may mediate their propensity for detachment. However, our present study was limited to biophysical (contraction and intracellular stress) and actin imaging analyses. Other approaches, such as RNA sequencing or proteomics assays, could elucidate intracellular pathways within stretched Actn4$^{K256E/K256E}$ podocytes that correspond with their biomechanical failure. Furthermore, the present model of periodic stretch (4 s of stretch followed by 3 min of recovery) is based on prior studies investigating the response to stretch of living adherent cells (16). However, podocytes in vivo experience more cyclic stretch at higher frequency with varying degrees of stretch. Brähler et al. (42) showed that podocyte oscillations were seen at the rate of the heartbeat. Finally, our study only examines stretch responsiveness in mutant podocytes cultured on flat 2D substrates. In vivo, the podocyte experiences fluid shear stress in addition to stretch as well as resides in complex 3D geometries (11). It would be important to incorporate these more realistic physical cues in future investigation.

Altogether, this study shows that the Actn4 mutation leads to a brittle podocyte whose structure and function fail under stretch. The presence of a K255E mutation in the actin-binding domain increases the affinity of the ACTN4 dimer to actin filaments. We now know that this not only alters the ACTN4–actin interaction and the behavior of cross-linked actin filaments in vitro but also alters the biomechanical behavior of glomerular podocytes in a well-defined manner. Podocytes expressing these mutant forms of Actn4 are brittle and demonstrate cytoskeletal failure after exposure to repeated stretch. The use of a point mutant mouse model confirms that these observations reflect the biology of native Actn4 rather than the effect of overexpression this protein. Thus, we can now make a direct connection from DNA mutation, to altered protein behavior, to a corresponding change in the podocyte's response to a mechanical challenge.

Materials and Methods

Please refer to *SI Materials and Methods* for detailed information regarding animal studies, cell isolation and imaging, biophysical measurements, and modeling. All animal procedures were approved by the Beth Israel Deaconess Medical Center (BIDMC) Animal Care and Use Committee.

ACKNOWLEDGMENTS. We thank Niccole Schaible and Justin Chun for help with the detachment assay. We thank Jae Hun Kim for his feedback with intracellular stress analysis. We thank Jeffrey Fredberg and Chan Y. Park for providing access and guidance for optical magnetic twisting microscopy measurements. We thank Clark DuMontier for assistance in data analysis, comments, and editing. This work was supported by NIH Grant R37DK59588 (to M.R.P.). D.F. was also supported by NIH Grant T32DK007199. We acknowledge the University of Alabama at Birmingham–University of California at San Diego, O'Brien Core (NIH Grant 1P30 DK 079337) for creatinine measurements. M. Bantawa, M. Bouzid, and E.D.G. acknowledge support from the Georgetown Environmental Initiative.

1. Saleem MA, et al. (2008) The molecular and functional phenotype of glomerular podocytes reveals key features of contractile smooth muscle cells. *Am J Physiol Renal Physiol* 295:F959–F970.
2. Neal CR, Crook H, Bell E, Harper SJ, Bates DO (2005) Three-dimensional reconstruction of glomeruli by electron microscopy reveals a distinct restrictive urinary subpodocyte space. *J Am Soc Nephrol* 16:1223–1235.
3. Welsh GI, Saleem MA (2011) The podocyte cytoskeleton—key to a functioning glomerulus in health and disease. *Nat Rev Nephrol* 8:14–21.
4. Kaplan JM, et al. (2000) Mutations in ACTN4, encoding alpha-actinin-4, cause familial focal segmental glomerulosclerosis. *Nat Genet* 24:251–256.
5. Weins A, et al. (2005) Mutational and biological analysis of alpha-actinin-4 in focal segmental glomerulosclerosis. *J Am Soc Nephrol* 16:3694–3701.
6. Choi HJ, et al. (2008) Familial focal segmental glomerulosclerosis associated with an ACTN4 mutation and paternal germline mosaicism. *Am J Kidney Dis* 51:834–838.
7. Feng D, Steinke JM, Krishnan R, Birrane G, Pollak MR (2016) Functional validation of an alpha-actinin-4 mutation as a potential cause of an aggressive presentation of adolescent focal segmental glomerulosclerosis: Implications for genetic testing. *PLoS One* 11:e0167467.
8. Ward SM, Weins A, Pollak MR, Weitz DA (2008) Dynamic viscoelasticity of actin cross-linked with wild-type and disease-causing mutant alpha-actinin-4. *Biophys J* 95: 4915–4923.
9. Yao NY, et al. (2011) Nonlinear viscoelasticity of actin transiently cross-linked with mutant α-actinin-4. *J Mol Biol* 411:1062–1071.
10. Ferrell N, et al. (2015) Shear stress is normalized in glomerular capillaries following ⅝ nephrectomy. *Am J Physiol Renal Physiol* 308:F588–F593.
11. Kriz W, Lemley KV (2015) A potential role for mechanical forces in the detachment of podocytes and the progression of CKD. *J Am Soc Nephrol* 26:258–269.
12. Endlich N, et al. (2001) Podocytes respond to mechanical stress in vitro. *J Am Soc Nephrol* 12:413–422.
13. Forst AL, et al. (2016) Podocyte purinergic P2X4 channels are mechanotransducers that mediate cytoskeletal disorganization. *J Am Soc Nephrol* 27:848–862.
14. Martineau LC, McVeigh LI, Jasmin BJ, Kennedy CR (2004) p38 MAP kinase mediates mechanically induced COX-2 and PG EP4 receptor expression in podocytes: Implications for the actin cytoskeleton. *Am J Physiol Renal Physiol* 286:F693–F701.
15. Morton MJ, et al. (2004) Human podocytes possess a stretch-sensitive, Ca^{2+}-activated K^+ channel: Potential implications for the control of glomerular filtration. *J Am Soc Nephrol* 15:2981–2987.
16. Trepat X, et al. (2007) Universal physical responses to stretch in the living cell. *Nature* 447:592–595.
17. Krishnan R, et al. (2009) Reinforcement versus fluidization in cytoskeletal mechanoresponsiveness. *PLoS One* 4:e5486.
18. Krishnan R, et al. (2012) Fluidization, resolidification, and reorientation of the endothelial cell in response to slow tidal stretches. *Am J Physiol Cell Physiol* 303: C368–C375.
19. Chen C, et al. (2010) Fluidization and resolidification of the human bladder smooth muscle cell in response to transient stretch. *PLoS One* 5:e12035.
20. Rosner SR, et al. (2017) The actin regulator zyxin reinforces airway smooth muscle and accumulates in airways of fatal asthmatics. *PLoS One* 12:e0171728.
21. Butler JP, Tolić-Nørrelykke IM, Fabry B, Fredberg JJ (2002) Traction fields, moments, and strain energy that cells exert on their surroundings. *Am J Physiol Cell Physiol* 282: C595–C605.
22. Wang N, et al. (2002) Cell prestress. I. Stiffness and prestress are closely associated in adherent contractile cells. *Am J Physiol Cell Physiol* 282:C606–C616.
23. Park CY, et al. (2010) Mapping the cytoskeletal prestress. *Am J Physiol Cell Physiol* 298: C1245–C1252.
24. Maruthamuthu V, Sabass B, Schwarz US, Gardel ML (2011) Cell-ECM traction force modulates endogenous tension at cell–cell contacts. *Proc Natl Acad Sci USA* 108: 4708–4713.
25. Tambe DT, et al. (2011) Collective cell guidance by cooperative intercellular forces. *Nat Mater* 10:469–475.
26. Tambe DT, et al. (2013) Monolayer stress microscopy: Limitations, artifacts, and accuracy of recovered intercellular stresses. *PLoS One* 8:e55172.
27. Trepat X, et al. (2009) Physical forces during collective cell migration. *Nat Phys* 5: 426–430.
28. Notbohm J, et al. (2016) Cellular contraction and polarization drive collective cellular motion. *Biophys J* 110:2729–2738.
29. Yao J, et al. (2004) Alpha-actinin-4-mediated FSGS: An inherited kidney disease caused by an aggregated and rapidly degraded cytoskeletal protein. *PLoS Biol* 2:e167.
30. Kos CH, et al. (2003) Mice deficient in alpha-actinin-4 have severe glomerular disease. *J Clin Invest* 111:1683–1690.
31. Galbraith CG, Yamada KM, Sheetz MP (2002) The relationship between force and focal complex development. *J Cell Biol* 159:695–705.
32. Gupta M, et al. (2015) Adaptive rheology and ordering of cell cytoskeleton govern matrix rigidity sensing. *Nat Commun* 6:7525.
33. Stamenović D, Wang N (2011) Stress transmission within the cell. *Compr Physiol* 1: 499–524.
34. Treloar KK, Simpson MJ (2013) Sensitivity of edge detection methods for quantifying cell migration assays. *PLoS One* 8:e67389.
35. Bouzid M, Del Gado E (October 4, 2017) Network topology in soft gels: Hardening and softening materials. *Langmuir*, 10.1021/acs.langmuir.7b02944.
36. Nagata M, Kriz W (1992) Glomerular damage after uninephrectomy in young rats. II. Mechanical stress on podocytes as a pathway to sclerosis. *Kidney Int* 42:148–160.
37. Ehrlicher AJ, et al. (2015) Alpha-actinin binding kinetics modulate cellular dynamics and force generation. *Proc Natl Acad Sci USA* 112:6619–6624.
38. Pagtalunan ME, et al. (1997) Podocyte loss and progressive glomerular injury in type II diabetes. *J Clin Invest* 99:342–348.
39. Wharram BL, et al. (2005) Podocyte depletion causes glomerulosclerosis: Diphtheria toxin-induced podocyte depletion in rats expressing human diphtheria toxin receptor transgene. *J Am Soc Nephrol* 16:2941–2952.
40. Vogelmann SU, Nelson WJ, Myers BD, Lemley KV (2003) Urinary excretion of viable podocytes in health and renal disease. *Am J Physiol Renal Physiol* 285:F40–F48.
41. Wickman L, et al. (2013) Urine podocyte mRNAs, proteinuria, and progression in human glomerular diseases. *J Am Soc Nephrol* 24:2081–2095.
42. Brähler S, et al. (2016) Intravital and kidney slice imaging of podocyte membrane dynamics. *J Am Soc Nephrol* 27:3285–3290.